MAP Estimation of Statistical Deformable Templates Via Nonlinear Mixed Effects Models: Deterministic and Stochastic Approaches

Stéphanie Allassonnière, Estelle Kuhn, Alain Trouvé

MAP Estimation of Statistical Deformable Templates Via Nonlinear Mixed Effects Models : Deterministic and Stochastic Approaches

Stéphanie Allassonnière[1], Estelle Kuhn[2], and Alain Trouvé[3]

[1] Center for Imaging Science, Johns Hopkins University, USA,
[2] LAGA, University Paris 13, France,
[3] CMLA, ENS Cachan, France,
stephanie@jhu.edu, kuhn@math.univ-paris13.fr, alain.trouve@cmla.ens-cachan.fr. *

Abstract. In [1], a new coherent statistical framework for estimating statistical deformable templates relevant to computational anatomy (CA) has been proposed. This paper addresses the problem of population average and estimation of the underlying geometrical variability as a MAP computation problem for which deterministic and stochastic approximation schemes have been proposed. We illustrate some of the numerical issues with handwritten digit and 2D medical images and apply the estimated models to classification through maximum likelihood.

1 Introduction

For the last decade, we are witnessing impressive achievements and the emergence of elaborated registration theories [2–4] but the definition of a proper statistical framework for designing and inferring stochastic deformable templates in a principled way is much less mature. Despite a seminal contribution [5] and the fact that deformable templates can be cast into the general Grenander's Pattern Theory [6], the down-to-earth and fundamental problem of computing *population averages* in presence of *unobserved* warping variables has not received so much attention from a more mathematical statistics perspective. More statistically oriented methods are slowly emerging [7–9] based on penalized likelihood or equivalently MDL approaches. Another line of research is to deal with the problem of population average as an estimation issue of proper stochastic (i.e. generative) models for which *consistency issues* should be addressed. In this direction, nonlinear mixed effects models (NLMM) are common tools in biostatistics and pharmacocinetic [10] to deal with both modelisation and inference of common *population factors* (fixed effects) and *distributions* of *unobserved* individuals factors (random effects). An active realm of research has emerged in the 90's for designing efficient and consistent estimation algorithms. The importation of such ideas even in the limited context of population average of grey level images in CA is extremely appealing and challenging –both theoretically

* We are thankful to Dr. Craig Stark for providing us with the medical data

and practically– because of the very large (virtually infinite) dimensionality of the related factors (common template and individual warpings). These new avenues have started to be explored and theoretically consistent procedures based on recent advances on stochastic approximation algorithms have been proposed in a series of papers [1, 11, 12]. Since these papers are mainly mathematically focussed papers, we would like in the present paper to address some of the numerical issues of the various "EM-like" algorithms proposed to numerically approximate the Maximum A Posteriori estimator. Some relevant results on the USPS database and 2D medical images are presented, showing the strength of such methods.

The paper is organized as follows. Sections 2, 3 and 4 respectively recall the mixture model and how the estimation is completed and the particular case of the one component model. The last section, Section 5, is devoted to the experiments.

2 The observation model: BME-Templates

Consider a population of n gray level images $(y_i(s))_{s\in\Lambda}$ defined on a discrete grid of pixels Λ and assume that each observation y derives from a noisy sampling at the pixels locations $(x_s)_{s\in\Lambda}$ of an *unobserved* deformation field $z : \mathbb{R}^2 \to \mathbb{R}^2$ of a *common* continuously defined template $I_0 : \mathbb{R}^2 \to \mathbb{R}$. This is what we call the Bayesian Mixed Effect Templates (BME-Templates). To keep things simple, we work within the small deformation framework [5] and assume that $y(s) = I_0(x_s - z(x_s)) + \sigma\epsilon(s) = zI_0(s) + \sigma\epsilon(s)$,where ϵ is a Gaussian normalized white noise and σ^2 is the common noise variance. The template I_0 and the deformation z are restricted to belong to subspaces of reproducing kernel Hilbert spaces V_p (resp. V_g) with kernel K_p (resp. K_g). Given $(p_k)_{1\le k\le k_p}$ a fixed set of landmarks covering the image domain, the template function I_0 is parameterized by coefficients $\alpha \in \mathbb{R}^{k_p}$ through: $I_\alpha = \mathbf{K_p}\alpha$, where $(\mathbf{K_p}\alpha)(x) = \sum_{k=1}^{k_p} K_p(x, p_k)\alpha(k)$. Similarly we write $z_\beta = \mathbf{K_g}\beta$ with another set of landmarks $(g_k)_{1\le k\le k_g}$ and a vector $\beta \in \mathbb{R}^{2k_g}$ of coefficients. In order to detect a global geometrical behavior, we consider the parameters β of the deformation field as an unobserved variable which is supposed to be Gaussian centered with covariance matrix Γ_g.

We present a general model based on NLMM defining a Bayesian mixture of m deformable template models (hereafter called components). In order to be able to consider small samples as our training sets, we have chosen to work within the Bayesian framework. In addition to the fact that some of the parameters, as the covariance matrix Γ_g, have been already used in many matching problems giving a first guess of what it could be, the Bayesian approach has its importance in the update formulas as a regularization term. This can particularly be noticed for Γ_g (cf [1]), where it always remains invertible in spite of the small sample size.

The model parameters of each component $t \in \{1, \dots, m\}$ are denoted by $\theta_t = (\alpha_t, \sigma_t^2, \Gamma_g^t)$. We assume that θ belongs to the open parameter space $\Theta \doteq \{\ \theta = (\alpha_t, \sigma_t^2, \Gamma_g^t)_{1\le t\le m} |\ \forall t \in \{1, \dots, m\}\ ,\ \alpha_t \in \mathbb{R}^{k_p},\ \sigma_t^2 > 0,\ \Gamma_g^t \in \Sigma^+_{2k_g,*}(\mathbb{R})\ \}$ and $\rho = (\rho_t)_{1\le t\le m}$ to the open simplex ϱ. Here $\Sigma^+_{2k_g,*}(\mathbb{R})$ is the set of strictly

For each component t (fixed effects) :

- ρ_t : probability of the component
- α_t : associated template parameter
- Γ_g^t : associated covariance matrix for deformation parameters
- σ_t^2 : associated additive noise variance

For each observation y_i (random effects) :

- τ_i : associated component
- β_i : deformation parameters
- ϵ_i : additive noise

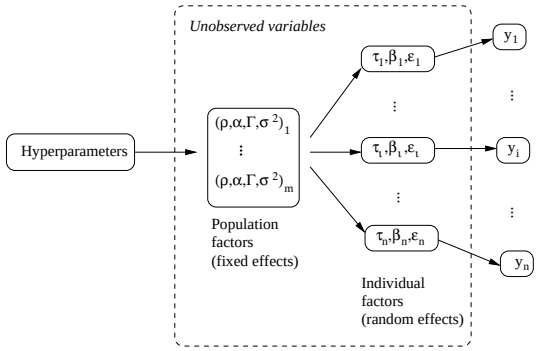

Fig. 1. Mixed effect structure for our BME-template

positive symmetric matrices. Let $\eta = (\theta, \rho)$, the precise hierarchical Bayesian structure of our model is :

$$\begin{cases} \rho \sim \nu_\rho \\ \theta = (\alpha_t, \sigma_t^2, \Gamma_g^t)_{1 \le t \le m} \sim \otimes_{t=1}^m (\nu_p \otimes \nu_g) \mid \rho \\ \tau_1^n \sim \otimes_{i=1}^n \sum_{t=1}^m \rho_t \delta_t \mid \rho \,, \\ \beta_1^n \sim \otimes_{i=1}^n \mathcal{N}(0, \Gamma_g^{\tau_i}) \mid \tau_1^n,\ \eta \\ y_1^n \sim \otimes_{i=1}^n \mathcal{N}(z_{\beta_i} I_{\alpha_i}, \sigma_{\tau_i}^2 Id_\Lambda) \mid \beta_1^n,\ \tau_1^n,\ \eta \end{cases}$$

with

$$\begin{cases} \nu_\rho(\rho) \propto \left(\prod_{t=1}^m \rho_t \right)^{a_\rho}, \\ \nu_p(d\sigma^2, d\alpha) \propto \left(\exp\left(-\frac{\sigma_0^2}{2\sigma^2} \right) \frac{1}{\sqrt{\sigma^2}} \right)^{a_p} \cdot \exp\left(-\frac{1}{2} \alpha^t (\Sigma_p)^{-1} \alpha \right) d\sigma^2 d\alpha, \\ \nu_g(d\Gamma_g) \propto \left(\exp(-\langle \Gamma_g^{-1}, \Sigma_g \rangle / 2) \frac{1}{\sqrt{|\Sigma_g|}} \right)^{a_g} d\Gamma_g, \end{cases}$$

where the hyper-parameters are fixed. All priors are the natural conjugate priors and assumed independent. A natural choice for the a priori covariance matrices Σ_p and Σ_g is to consider the matrices induced by the metric of the spaces V_p and V_g. Define the square matrices $M_p(k,k') = K_p(p_k, p_{k'})\ \forall 1 \le k, k' \le k_p$ and $M_g(k,k') = K_g(g_k, g_{k'})\ \forall 1 \le k, k' \le k_g$, and then set $\Sigma_p = M_p^{-1}$ and $\Sigma_g = M_g^{-1}$, which are typical prior matrices used in many matching algorithms.

3 Estimation of the parameters

The parameter estimates are obtained by maximizing the posterior density on η conditional on y_1^n: $\hat{\eta}_n = \text{argmax}_\eta\, q(\eta | y_1^n)$. Since the deformation coefficients β_1^n and component labels τ_1^n are unobserved, the natural approach is to use iterative algorithms such as EM [13] to maximize the penalized likelihood given

the observations y_1^n. This likelihood is written as an integral over the hidden variables, making the direct maximization a difficult task. The EM algorithm consists in an iterative procedure to solve this problem. Each iteration of the algorithm is divided into two steps; let l be the current iteration:

E Step: Compute the posterior law on (β_1^n, τ_1^n) as the following distribution:

$$\nu_l(\beta_1^n, \tau_1^n) \propto \prod_{i=1}^{n} q(y_i|\beta_i, \alpha_{\tau_i,l}) q(\beta_i|\Gamma_{g,l}^{\tau_i}) \rho_{\tau_i,l}$$

M Step: $\eta_{l+1} = \text{argmax}_\eta \, E_{\nu_l}[\log q(y_1^n, \beta_1^n, \tau_1^n, \eta)]$.

In the present context, we initialize the algorithm with the prior model η_0.

3.1 Fast approximation with modes (FAM)

The expression in the M step requires the computation of the expectation with respect to the posterior distribution of $\beta_1^n, \tau_1^n | y_1^n$, computed in the E step, which is known here up to the re-normalization constant. To overcome this obstacle, given an observation y_i and a label t, the posterior distribution of the random deformation field is approximated at iteration l by a Dirac law on its mode $\beta_{l,i,t}^*$. This yields the following computation :

$$\begin{aligned}\beta_{l,i,t}^* &= \arg\max_\beta \log q(\beta|\alpha_{t,l}, \sigma_{t,l}^2, \Gamma_{g,l}^t, y_i) \\ &= \arg\min_\beta \left\{ \frac{1}{2}\beta^t (\Gamma_{g,l}^t)^{-1} \beta + \frac{1}{2\sigma_{l,t}^2} |y_i - K_p^\beta \alpha_{t,l}|^2 \right\},\end{aligned}$$

which is a standard template matching problem with the current parameters. We then approximate the joint posterior on (β_i, τ_i) as a discrete distribution concentrated at the m points $(\beta_{l,i,t}^*)_{1 \le t \le m}$ with weights given by: $w_{l,i}(t) \propto q(y_i|\beta_{l,i,t}^*, \alpha_{t,l}) q(\beta_{l,i,t}^*|\Gamma_{g,l}^t) \rho_{t,l}$. The label $\tau_{l,i}$ is then sampled from the distribution $\sum_{t=1}^m w_{l,i}(t)\delta_t$ and the deformation is the mode of the drawn label $\beta_{l,i} = \beta_{l,i,\tau_i}^*$.

The maximization is then done on this approximation of the likelihood.

3.2 Using a stochastic version of the EM algorithm : SAEM-MCMC

An alternative to the computation of the E-step in a complex nonlinear context is to use the stochastic approximation EM algorithm (SAEM) [14] coupled with an MCMC procedure [15] and a truncation on random boundaries. Our model belongs to the exponential density family which means that: $q(y, \beta, \tau, \eta) = \exp\left[-\psi(\eta) + \langle S(\beta, \tau), \phi(\eta)\rangle\right]$, where the sufficient statistic S is a Borel function on $\mathbb{R}^{2k_g} \times \{1, \ldots, m\}$ taking its values in an open subset $\mathcal{S}$ of $\mathbb{R}^m$ and ψ, ϕ two Borel functions on $\Theta \times \varrho$ (the dependence on y is omitted for sake of simplicity).

We introduce the following function: $L : \mathcal{S} \times \Theta \times \varrho \to \mathbb{R}$ as $L(s; \eta) = -\psi(\eta) + \langle s, \phi(\eta)\rangle$. Direct generalisation of the proof in [1] to the multicomponent model

gives the existence of a critical function $\hat{\eta} : \mathcal{S} \to \Theta \times \varrho$ which satisfies: $\forall \eta \in \Theta \times \varrho, \forall s \in \mathcal{S}, L(s; \hat{\eta}(s)) \geq L(s; \eta)$. Then, iteration l of this algorithm consists of the following four steps.

Simulation step: The missing data are drawn using a transition probability of a convergent Markov chain having the posterior distribution as stationary distribution: $(\beta_{l+1}, \tau_{l+1}) \sim \Pi_{\eta_l}((\beta_l, \tau_l), \cdot)$

Stochastic approximation step: Since the model is exponential, the stochastic approximation is done on the sufficient statistics using the simulated values of the missing data: $s_{l+1} = s_l + \Delta_{l+1}(S(\beta_{l+1}, \tau_{l+1}) - s_l)$,where $(\Delta_l)_l$ is a decreasing sequence of positive step-sizes.

Truncation step: A truncation is done on the stochastic approximation.

Maximization step: The parameters are updated: $\eta_{l+1} = \hat{\eta}(s_{l+1})$.

Concerning the choice of Π_η used in the simulation step, as we aim to simulate (β_i, τ_i) through a transition kernel whose stationary distribution is $q(\beta, \tau | y_i, \eta)$, we simulate τ_i with a kernel whose stationary distribution is $q(\tau | y_i, \eta)$ and then β_i through a transition kernel that has $q(\beta | \tau, y_i, \eta)$ as stationary distribution. Given any initial deformation field $\xi_0 \in \mathbb{R}^{2k_g}$, we run, for each component t, J_l iterations of a hybrid Gibbs sampler (for each coordinate of the vector, a Hasting-Metropolis sampling is done given the other coordinates) $\Pi_{\eta,t}$ using the conditional prior distribution $\beta^j | \beta^{-j}$ as the proposal for the j^{th} coordinate, β^{-j} referring to β without its j^{th} coordinate. So that we get J_l elements $\xi_{t,i} = (\xi_{t,i}^{(k)})_{1 \leq k \leq J_l}$ of an ergodic homogeneous Markov chain whose stationary distribution is $q(\cdot | y_i, t, \eta)$. Denoting $\xi_i = (\xi_{t,i})_{1 \leq t \leq m}$, we simulate τ_i through the discrete density with weights given by: $\hat{q}_{\xi_i}(t | y_i, \eta) \propto \left(\frac{1}{J_l} \sum_{k=1}^{J_l} \left[\frac{f_t(\xi_{t,i}^{(k)})}{q(y_i, \xi_{t,i}^{(k)}, t | \eta)} \right] \right)^{-1}$,where f_t is the density of the Gaussian distribution $\mathcal{N}(0, \Gamma_{g,t})$. Then, we update β_i by rerunning J_l times the hybrid Gibbs sampler Π_{η, τ_i} starting from a random initial point β_0. It has been proved in [12], that the sequence $(\eta_l)_l$ generated through this algorithm converges a.s. toward a critical point of the penalized likelihood of the observations.

4 Single component model

We focus here on the single component model ($m = 1$). The unobserved variables are only the deformation fields β and the parameters are reduced to $\theta = (\alpha, \sigma^2, \Gamma_g)$. In this particular setting, denoting by P the distribution governing the observations and by $\Theta_* = \{ \theta_* \in \Theta \mid E_P(\log q(y | \theta_*)) = \sup_{\theta \in \Theta} E_P(\log q(y | \theta)) \}$, it has been proved in [1] that the MAP estimator $\hat{\theta}_n$ exists a.s. and converges toward an element in Θ_*. From the algorithmical viewpoint, the FAM algorithm does not require any changes. Indeed, each E step only corresponds to a single computation of the mode of the posterior density. However, the stochastic algorithm can be simplified. In the simulation step, only a single iteration of the Markov chain (i.e. $J_l = 1$, $\forall l$) is needed for each iteration of the SAEM algorithm: $\beta_{l+1} \sim \Pi_{\theta_l}(\beta_l, \cdot)$ yielding a non homogeneous Markov chain. It has been

proved in [11], that the sequence $(\theta_l)_l$ generated converges almost surely toward a critical point of the penalized likelihood of the observations.

5 Experiments

5.1 Estimation results

We illustrate this theoretical framework with the USPS handwritten digit database which corresponds to non noisy gray level images. In addition, we compare the two algorithmical approaches on 2D medical images of the corpus calosum (the splenium) and a part of the cerebellum.

Figure 2 shows the templates estimated from a training set (Figure 2-(a)) of 20 or 40 images per digit with both algorithms for the models with one and two components per class respectively. The results are quite similar, in particular the two components present the same features for both algorithms. Topologically different shapes are separated (cf digits 7 and 2) and the other digit clusters are relevant. While estimating a single component, the templates are good representatives of the shapes existing in the training set.

Concerning the geometrical variability, Figure 3, left image, presents some synthetic examples drawn with respect to the model with the estimated parameters. In spite of some artefacts described below, the kind of deformations learnt applied to the estimated templates looks like the elements of the training set which means that the algorithms capture this geometrical variability.

Last but not least, one could wonder how those algorithms deal with noisy images. In [1], this particular case has been shown to fail with the FAM algorithm with a toy example. Whereas, in [11, 12], the authors have proved the theoretical convergence of the two stochastic algorithms (for the mixture and simple models). This supports the fact that the estimated parameters should be less sensitive to the noise that can appear in the data. This is what we show in Figure 1 for a database of 20 images per digit which is partly presented (a). The results are related to the theory. Indeed, the FAM algorithm is stuck in

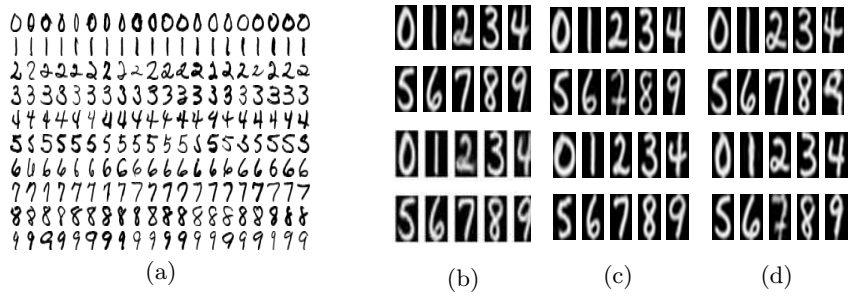

(a) (b) (c) (d)

Fig. 2. (a) Some images of the USPS training set: 20 images per class. (b,c,d): Top row : FAM Algorithm, Bottom row : SAEM-MCMC algorithm. (b): one component prototype. (c-d): 2 component prototypes.

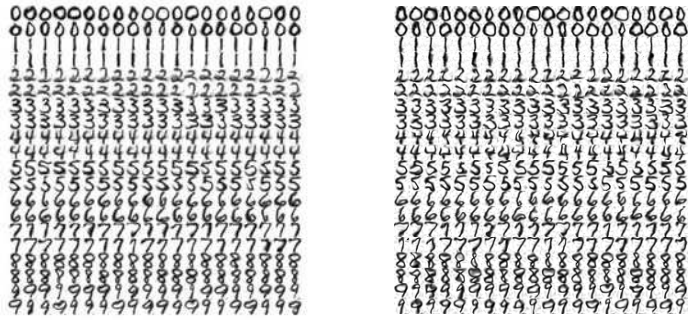

Fig. 3. 40 synthetic examples per class generated with the estimated parameters: 20 with the direct deformations and 20 with the inverse deformations. Left: from the non-noisy database estimated parameters. Right: from the noisy database estimated parameters. Note that the variability of digit is well reproduced, both in the case of highly deformable digits (e.g. 2 and 4) or in more constrained situations (e.g. 7 and 1).

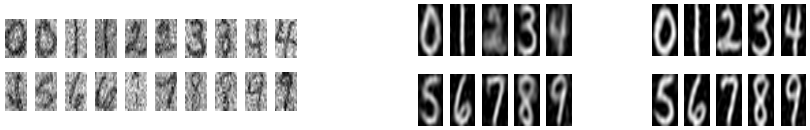

(a) (b) (c)

Fig. 4. (a) Two images per digit of the noisy database. (b) Estimated prototypes in a noisy setting $\sigma^2 = 1$. (c) with the FAM algorithm. Right : with the SAEM-MCMC coupling procedure.

some local maximum of the likelihood (b) whereas the stochastic algorithm (c) reaches a better estimator for the parameters. This illustrates the power of the stochastic approach to solve this problem. Both the template and the geometrical distribution are well estimated. The results are presented in Figure 4 and in the right image of Figure 3 where we can notice that the estimation of the photometrical and the geometrical variability is quite robust to addition of a significant amount of noise.

The computational times of both algorithms for the simple model are very similar. The gradient descent required to compute the mode at each iteration lasts as long as one run of the Gibbs sampler used in the simulation step. The estimation takes only a couple of minutes on this dataset. For the general model, the SAEM-MCMC algorithm takes longer (increasing linearly with the number of component times the number of iterations of the Gibbs sampler J_l) since it requires the computation of many iterations of m Markov chains which can

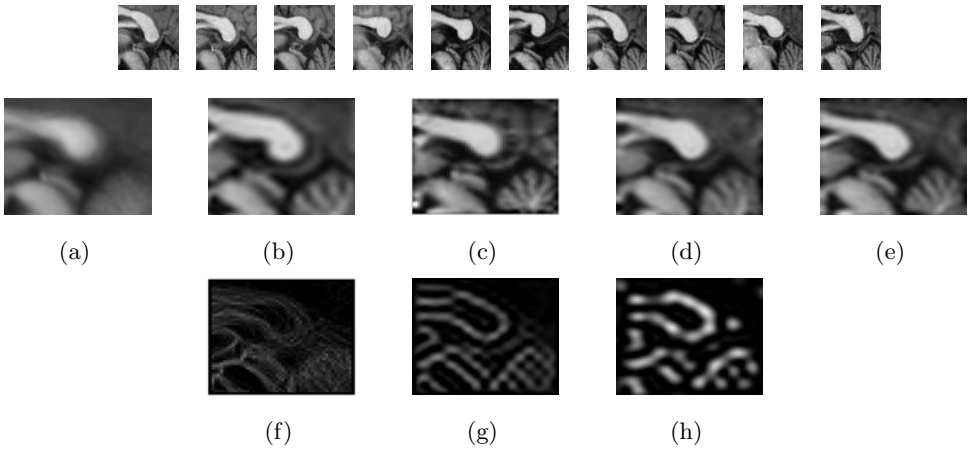

Fig. 5. First row : Ten images of the training set representing the splenium and a part of the cerebellum. Second row : Results from the template estimation. (a) : gray level mean image of the 47 images. Templates estimated (b) : with the FAM (c) : with the stochastic algorithms on the simple model (d,e) : on the two component model. Third row : (f,g,h) : gray level mean image of the 47 images of the edges and estimated templates with the FAM and the stochastic algorithm on the simple model.

actually be easily parallelized. In addition, the number J_l of iterations of the Markov chain can be fixed all along the algorithm in the experiments.

We also test the algorithms on some medical images. The database we consider has 47 2D images, each of them representing the splenium (back of the corpus calosum) and a part of the cerebellum. Some of the training images are shown in Figure (5) first row.

The results of the estimation are presented in Figure 5 where we can see the improvement from the gray level mean (a) to our estimations. Image (b), corresponding to the deterministic algorithm result, shows a well contrasted splenium whereas the cerebellum remains a little bit blurry (note that it is still much better that the simple mean). Image (c), corresponding to the stochastic EM algorithm result, presents some real improvement again. Indeed, the splenium is still very contrasted, the background is not blurry and overall, the cerebellum is well reconstructed with several branches. The two anatomical shapes are relevant representants of the ones observed in the training set.

The estimation has been done while enabling the decomposition of the database into two components. The two estimated templates (using the MCMC-SAEM algorithm) are presented in Figure 5 (d) and (e). The differences can be seen in particular on the shape of the splenium, where the fornix is more or less close to the boundary of the image and the thickness of the splenium varies. The number of branches in the two cerebella also tends to be different from one template to the other (4 in the first component and 5 in the second one). The estimation suffers from the small number of images we have. To be able to explain the huge

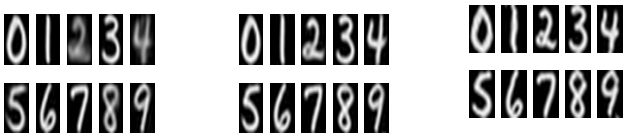

Fig. 6. Estimated prototypes (20 images per digit), $\sigma_g = 0.2$ (Left), $\sigma_g = 0.3$ (Right) with images in $[-1, 1]^2$.

variability of the two anatomical shapes, more components would be interesting but at the same time more images required so that the components will not end up empty.

To emphasize the robustness of both algorithms, we run them on some binary images representing the edges of the same medical images. The exact same parameters are used and the results are shown in Figure 5, third row. Whereas the gray level mean image (f) does not represent any relevant information about the edges of the anatomical shapes, the FAM algorithm (g) tends to model the splenuim and some branches of the cerebellum. Nevertheless, it does not lead to very contrasted shape boundaries as captured by the stochastic EM approach (h).

5.2 Optimization on the representation, model and algorithms

Despite the fact that many parameters (e.g. the noise variance) are self-calibrated during the estimation process, the algorithm depends on some hyper-parameters we would like to discuss briefly.

Data representation issues. The first point to be explained is the effect of the representation of the data, in particular the spline representation of both the template and the deformations (cf Section 2). We have chosen Gaussian kernels. The influence of their two scales can be seen on the template estimation. Indeed, choosing a too small geometric scale leads to very localized deformations around *fixed* control points and the resulting template is more blurry. In Figure 6, we present the results on a 20 handwritten digit images learning process. On the opposite side, a very large scale induces very smooth deformations which would no longer be relevant for the kind of deformations required to explain the database.

Concerning the photometric scale, it is straightforward that a large scale will drive to blurry template. This is particularly noticeable on digit 1 where the thickness significantly increases (cf Figure 7 two left images).

In addition, the effects of increasing scale can also be noticed on the learnt covariance matrix. Given a fatty template, the deformations required to fit the database will be forced to contract the template. This phenomena is thus important in the learnt covariance matrix. When we generate new data thanks to the estimated parameters, we can see, as in Figure 7 right images, that the template

is contracted, which is relevant, but also enlarged since the distribution on β is symmetric (this particular point is detailed in the next paragraph). Those large images are not typical from the training set.

Model distribution issues. One question is the relevance of the Gaussian distribution chosen for the deformation field. It is natural to think that the mean of the deformations around an atlas is close to zero whereas the symmetry of the distribution (the probability of a deformation field + β equals its opposite one $-\beta$) is much more arguable. In Figure 3, we show the effects of the action of both fields on the learnt 10 digits templates. For example, digits 3 and 9 present, for some generated examples, irregular images whereas the opposite deformation leads to an image which is very similar to one or more element of the training set. Another distribution should be considered in future work.

Another issue about the model is the choice of the prior hyper-parameters. In particular, the effect of the inverse Wishart prior a_g on the geometric covariance matrix is important. Indeed, if we want to satisfy the theoretical requirements to the algorithms, we have to chose $a_g \geq 4k_g + 1$. However, the update formula is a barycenter between the expectation of the empirical covariance matrix and the prior with weights n and a_g respectively (cf: [1]). Since we are working with small sample sizes, this condition makes the update of Γ_g very constrained close to the prior Σ_g. This does not enable the geometry to be well estimated and the effects can be seen directly on the template but also on the classification rate [1]. The value of a_g used in those particular experiments is fixed to 0.5. Concerning the other weights (a_p, a_ρ), their effects are less significant on the results and we fixed them to 200 and 2 respectively.

Stochastic algorithm issues. The FAM algorithm is deterministic and does not depend on any choice. Unfortunately, the stochastic algorithm requires several choices to optimize.

To optimize the choice of the transition kernel Π_η, we run the algorithm with different kernels and compare the evolution of the simulated hidden variables as well as the results on the estimated parameters. Some kernels, as an ordinary Hastings Metropolis algorithm using as proposal the prior or a standard random walk added to the current value, do not allow to visit well the entire support of the unobserved variable. From this point of view the hybrid Gibbs sampler we used has better properties and gives nice estimation results.

Fig. 7. Two left images: Estimated prototypes of digit 1 (20 images per class) for different hyper-parameters. Left: smaller geometry and larger photometric scales. Right: larger geometry and smaller photometric scales. Right images: Synthetic examples corresponding respectively to the two previous templates of digit 1.

To prove the convergence of the stochastic algorithms, we have to suppose that as soon as the stochastic approximation wanders outside an increasing compact set, the unobserved variable needs to be projected inside a given compact set (this is the truncation on random boundaries). In practice however, this step is never required, the results presented were obtained without this control.

Finally, the initialization of the parameters can lead to undesirable effects. For example, if the first value of the photometric parameter α is set to 0, at the first iteration of the Gibbs sampler, the proposal will be accepted with probability one. Since the candidate coordinates are simulated according to the conditional a priori, the resulting vector β leads to a variation which does not correspond to a relevant digit deformation. This implies some oscillations on the updated template. The next simulated deformation variable will try to take these oscillations into account to get closer and closer to the oscillating template, staying in its orbit. The results can be observed in Figure 6 (Right) specially for digit 1.

5.3 Results on classification rates

To get an objective way of comparing our algorithms and showing their performances, we use our model to propose a classifier which can easily be run on the USPS test set. We use the same approximations for the classification process, either a mode approximation of the posterior density or some MCMC methods to approximate the expectation required to compute the best class. Running the estimation with a FAM algorithm on all USPS database with 15 components and using a "mode" classifier gives a classification error rate of 3.5%. This is comparable to other classifiers results. The importance of the coupled photometric and geometric estimation is emphasized in [1].

Since the drawback of this method can be better proved in the presence of noise, we add an independent Gaussian noise of variance 1 on both the training set and the test set and run both estimations (with one component and 20 images per class) and both classifications. We run the parameter estimation though the "SAEM-like" algorithm presented in the previous section and test the model with these estimated parameters as a classifier. The classification error rate obtained are 22.52% when the classification uses the mode approximation and 17.07% using some MCMC methods. These results are a lot worse if the parameters are estimated with the FAM algorithm. For example, the classification error reaches 40.71% when the classification is done via the mode approximation as well.

6 Conclusion

We have presented some applications of the coherent statistical framework with BME-Template models described in [1, 11, 12]. This framework is fairly versatile and could be derived in many other important situations in CA. The possibility to work with mixture of deformable templates in a principled statistical way is also a quite enjoyable and unique feature of this setting. Reported experiments show that the deterministic FAM algorithm, despite its simplicity, performed

significantly worse especially under noisy conditions than the more sophisticated stochastic alternative. The introduction of such MCMC methods are still quite challenging in the 3D setting or for large deformation ([16] for a "FAM like" template estimation) but from an algorithmic point of view, there is a continuous interpolation from deterministic to stochastic algorithms (just increasing the number of MCMC steps) so that there is no sharp complexity gaps between to two approaches. Increasingly available computational power will make such stochastic approaches more and more appealing in the future.

References

1. Allassonnière, S., Amit, Y., Trouvé, A.: Toward a coherent statistical framework for dense deformable template estimation. J.R.S.S. **69** (2007) 3–29
2. Toga, W.A., Thompson, P.M.: The role of image registration in brain mapping. Image and Vision Computing Journal **19**(1–2) (2001) 3–24
3. Miller, M.I., Younes, L.: Group actions, homeomorphisms, and matching: A general framework. Int. J. Comput. Vision **41**(1-2) (2001) 61–84
4. Miller, M.I., Trouvé, A., Younes, L.: Geodesic shooting for computational anatomy. J. Math. Imaging Vision **24** (2006) 209–228
5. Amit, Y., Grenander, U., Piccioni, M.: Structural image restoration through deformable templates. JASA **86** (1991) 376–387
6. Grenander, U., Miller, M.: Pattern theory: from representation to inference. Oxford; New York: Oxford University Press (2007)
7. Glasbey, C.A., Mardia, K.V.: A penalised likelihood approach to image warping. Journal of the Royal Statistical Society, Series B **63** (2001) 465–492
8. Marsland, S., Twining, C.J., Taylor, C.J.: A minimum description length objective function for groupewise non-rigid image registration. Im. Vis. Comp. (2007)
9. Van Leemput, K.: Probabilistic Brain Atlas Encoding Using Bayesian Inference. MICCAI **1** (2006) 704–711
10. Lindstrom, M., Bates, D.: Nonlinear mixed effects models for repeated measures data. Biometrics **46**(3) (1990) 673–687
11. Allassonnière, S., Kuhn, E., Trouvé, A.: Bayesian deformable models building via stochastic approximation algorithm: A convergence study. in revision
12. Allassonnière, S., Kuhn, E.: Stochastic algorithm for parameter estimation for dense deformable template mixture model. submitted
13. Dempster, A.P., Laird, N.M., Rubin, D.B.: Maximum likelihood from incomplete data via the EM algorithm. Journal of the Royal Statistical Society **1** (1977) 1–22
14. Delyon, B., Lavielle, M., Moulines, E.: Convergence of a stochastic approximation version of the EM algorithm. Ann. Statist. **27**(1) (1999) 94–128
15. Kuhn, E., Lavielle, M.: Coupling a stochastic approximation version of EM with an MCMC procedure. ESAIM Probab. Stat. **8** (2004) 115–131 (electronic)
16. Ma, J., Miller, M., Trouvé, A., Younes, L.: Bayesian template estimation in computational anatomy. To appear in NeuroImage (2008)